Geoengineering impact of open ocean dissolution of olivine on atmospheric CO_2, surface ocean pH and marine biology

Geoengineering impact of open ocean dissolution of olivine on atmospheric CO₂, surface ocean pH and marine biology

Peter Köhler, Jesse F Abrams[1], Christoph Völker, Judith Hauck and Dieter A Wolf-Gladrow

Alfred Wegener Institute for Polar and Marine Research (AWI), PO Box 12 01 61, D-27515 Bremerhaven, Germany

E-mail: Peter.Koehler@awi.de

Abstract
Ongoing global warming induced by anthropogenic emissions has opened the debate as to whether geoengineering is a 'quick fix' option. Here we analyse the intended and unintended effects of one specific geoengineering approach, which is enhanced weathering via the open ocean dissolution of the silicate-containing mineral olivine. This approach would not only reduce atmospheric CO₂ and oppose surface ocean acidification, but would also impact on marine biology. If dissolved in the surface ocean, olivine sequesters 0.28 g carbon per g of olivine dissolved, similar to land-based enhanced weathering. Silicic acid input, a byproduct of the olivine dissolution, alters marine biology because silicate is in certain areas the limiting nutrient for diatoms. As a consequence, our model predicts a shift in phytoplankton species composition towards diatoms, altering the biological carbon pumps. Enhanced olivine dissolution, both on land and in the ocean, therefore needs to be considered as ocean fertilization. From dissolution kinetics we calculate that only olivine particles with a grain size of the order of 1 μm sink slowly enough to enable a nearly complete dissolution. The energy consumption for grinding to this small size might reduce the carbon sequestration efficiency by ∼30%.

Keywords: geoengineering, carbon cycle, marine biology, olivine, enhanced weathering, ocean alkalinization, ocean fertilization

S Online supplementary data available from stacks.iop.org/ERL/8/014009/mmedia

1. Introduction

The Earth's climate is currently perturbed by anthropogenic impacts. The rise in atmospheric CO₂ concentration caused by burning of fossil fuels and land use change leads not only to a global temperature increase, but also to other adverse effects such as ocean acidification (Doney *et al* 2009). Over the coming century, most IPCC emission scenarios (Joshi *et al* 2011, Rogelj *et al* 2011) will lead to a global warming larger than 2 K, the limit that was set by the United Nations Framework Convention on Climate Change in Copenhagen in 2009 (UNFCCC 2009). To prevent Earth's climate from crossing this 2 K threshold atmospheric CO₂ must be stabilized below approximately 450–500 μatm. This requires massive reduction in future CO₂ emissions in the present century (Meinshausen *et al* 2009, Solomon

[1] Present address: Leibniz-Zentrum für Marine Tropenökologie (ZMT) GmbH, Fahrenheitstraße 6, D-28359 Bremen, Germany.

et al 2009) and even negative emissions over the next millennium (Friedlingstein *et al* 2011). In light of these circumstances, geoengineering is discussed as potentially being of use as a relatively quick fix against these warming trends. Various geoengineering concepts relying on either solar radiation management or carbon dioxide removal (CDR) were proposed (Lenton and Vaughan 2009, The Royal Society 2009). CDR approaches remove CO_2 from the atmosphere/surface ocean and might also address surface ocean acidification, although some approaches re-locate the acidification problem to the seafloor (Williamson and Turley 2012).

Enhanced silicate weathering—here by the dissolution of the silicate-containing mineral olivine—is one of the CDR approaches. It should be mentioned that enhanced carbonate weathering (Kheshgi 1995, Caldeira and Rau 2000, Harvey 2008, Rau 2008, 2011) is an alternative CDR approach which will not be discussed any further here. Olivine dissolution is part of the natural silicate weathering process, which reduced atmospheric CO_2 over geological timescales in the past (Berner 1990). Olivine (Mg_2SiO_4) is an abundantly available magnesium silicate which weathers according to the reaction (Schuiling and Krijgsman 2006)

$$(Mg, Fe)_2SiO_4 + 4\,CO_2 + 4H_2O \Rightarrow 2(Mg, Fe)^{2+}$$
$$+ 4\,HCO_3^- + H_4SiO_4. \quad (1)$$
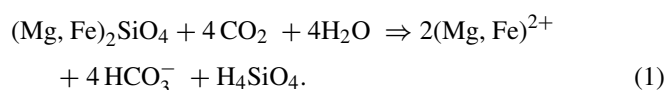
The abundance of Mg compared to Fe depends on the rock, but is about 90% in the well abundant dunite (Deer *et al* 1992). This net dissolution reaction suggests that 1 mole of olivine would sequester 4 moles of CO_2, equivalent to sequestration rates of 0.34 g C per g olivine. It has been shown that those are theoretical upper limits, and the effect of the ocean's carbon chemistry lead to 20% smaller sequestration rates (Köhler *et al* 2010). The dissolution of one mole of olivine leads in the surface ocean to an increase in total alkalinity by 4 moles and in silicic acid (H_4SiO_4) by one mole, the latter is a limiting nutrient for diatoms in large sections of the world's oceans (Nelson *et al* 1995, Dugdale and Wilkerson 1998, Ragueneau *et al* 2006). Present day input of silicate (SiO_4) due to natural riverine fluxes (Beusen *et al* 2009), which account for 80% of silicate flux into the ocean (Tréguer and De La Rocha 2013), is 380 Tg Si yr^{-1} or 6 Tmol Si yr^{-1}. The Si input into the ocean would be increased by 7 Tmol Si yr^{-1} per Pg of olivine dissolved. Recently, the geoengineering potential of enhanced silicate weathering on land has been evaluated (Köhler *et al* 2010). They calculated that olivine distributed as fine powder over land areas of the humid tropics has the potential to sequester up to 1 Pg C yr^{-1}, but is limited by the saturation concentration of silicic acid in rivers and streams. Here we extend the olivine dissolution scenarios from land to open ocean. We calculate for the first time not only the intended effects, but also some unintended side effects of olivine dissolution in the open ocean on atmospheric CO_2, surface ocean pH and on the marine biology with a marine ecosystem model embedded in an ocean general circulation model. Our results also have implications for the land-based approach of enhanced weathering.

2. Methods

To explore the effectiveness of the enhanced weathering of olivine, we use the biogeochemical model REcoM-2 coupled to the Massachusetts Institute of Technology general circulation model (MITgcm). MITgcm (Marshall *et al* 1997) is configured globally, excluding the Arctic Ocean north of 80°N, with a longitudinal spacing of 2° and a latitudinal spacing that varies from 1/3° to 2°, with a higher resolution around the equator to account for the equatorial undercurrent and to avoid nutrient trapping (Aumont *et al* 1999). Additionally, in the Southern Hemisphere the latitudinal resolution is scaled by the cosine of the latitude, to ensure an isotropic grid spacing even near the Antarctic continent. The model setup consists of 30 vertical levels, whose thickness increases from 10 m at the surface to 500 m in the deep ocean. A thermodynamic and dynamic sea-ice model is applied (Losch *et al* 2010).

The REcoM (Schartau *et al* 2007) (regulated ecosystem model) ecosystem and biogeochemistry model allows for changes in phytoplankton C:N:Chl stoichiometry in response to light, temperature and nutrient availability (Geider *et al* 1998). REcoM-2 allows for two phytoplankton species types: diatoms and nanophytoplankton. The current version of the model, and the applied forcing together with a validation of the model's biogeochemical fields are described in detail elsewhere (Hauck 2012). The model structure is outlined in figure S1 (available at stacks.iop.org/ERL/8/014009/mmedia). The model setup differs from that used previously (Hauck 2012) in one detail, namely a slightly changed parameterization of the formation of $CaCO_3$ by nanophytoplankton. This difference leads to somewhat higher alkalinity near the surface in (Hauck 2012) than here. The model is spun up for a period of 100 yr from 1900 to 1999, and then integrated from 2000 to the end of 2009 with and without olivine input. The period from 1900 to 1947 is forced with the climatological CORE data set (Large and Yeager 2008). The period from 1948 to 2009 is forced with daily fields from the NCEP/NCAR-R1 data (Kalnay *et al* 1996). In the model we use a prescribed atmospheric CO_2. Before 1958, the CO_2 values are derived from a spline fit (Enting *et al* 1994) to ice core data (Neftel *et al* 1985) and recent direct measurements. After 1958, annual averages of atmospheric CO_2 from Mauna Loa are used (Keeling *et al* 2009).

We employed a non-interactive atmospheric pCO_2. Neglecting the feedback of an interactive atmospheric CO_2 as done here may lead to an overestimation of the oceanic carbon uptake and inventory. The reference run without olivine dissolution (CONTROL) is described in detail in the supplementary data and figure S2 (available at stacks.iop.org/ERL/8/014009/mmedia). The dissolution of 1 mole of olivine was simulated via the input of 4 moles of total alkalinity (TA) and/or 1 mole of silicic acid (Si) into the surface ocean (equation (1)). Increased alkalinity for constant dissolved inorganic carbon leads to a reduction of the concentration of CO_2 in the surface water (Zeebe and Wolf-Gladrow 2001), followed by oceanic CO_2 uptake from the atmosphere via gas exchange. We use 140 g as molar weight of olivine implying
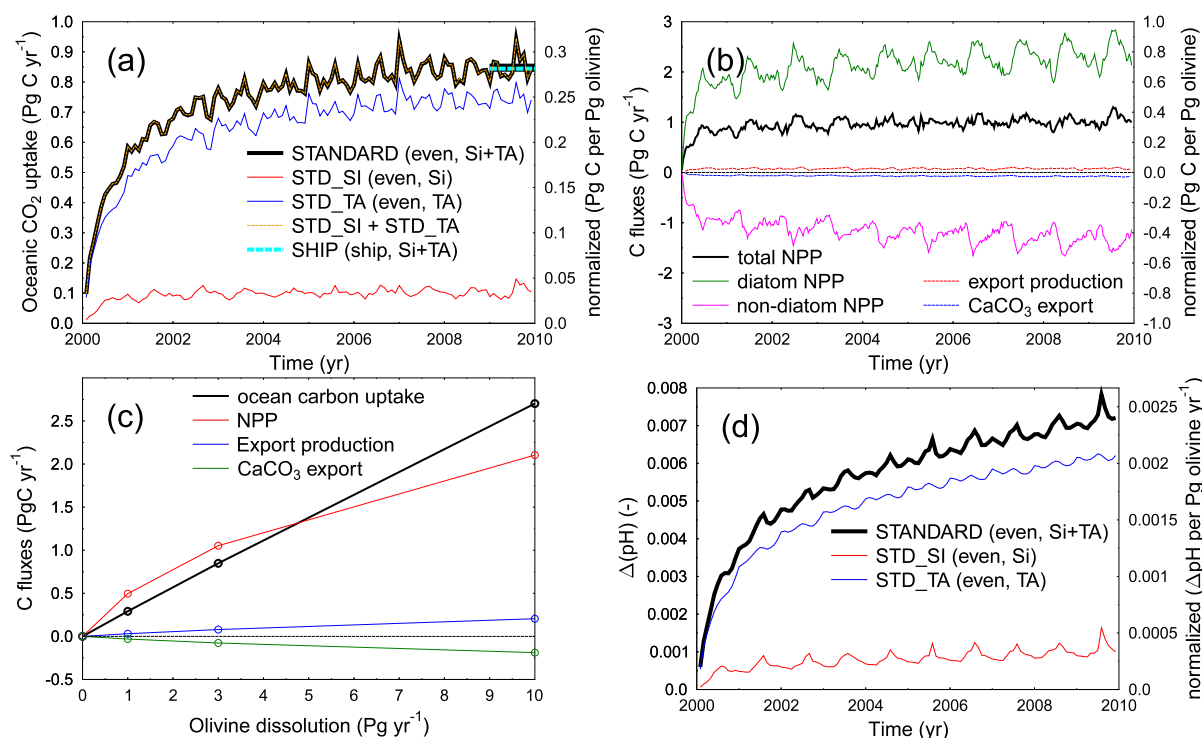
Figure 1. Main simulation results. (a) The temporal evolution of the oceanic carbon uptake compared to CONTROL for all distribution scenarios. The short lines in year 2009 are the values for the annual mean in 2009 for scenarios STANDARD and SHIP. (b) The temporal evolution of the response of the ocean's biology (total, diatom and non-diatom NPP, export production (of organic carbon) and of $CaCO_3$ out of the surface ocean) to olivine distribution for scenario STANDARD with respect to CONTROL. (c) Oceanic carbon uptake, total NPP, export production of organic carbon and of $CaCO_3$ out of the surface ocean as a function of the amount of olivine dissolution (scenarios SMALL, STANDARD and LARGE with 1, 3, 10 Pg of olivine dissolution per year, respectively). Plotted are averages over the final year 2009. (d) The temporal evolution of the accumulated change in mean sea surface pH.

that the dissolved olivine contains only Mg and no Fe. The fluxes of TA and Si are evenly distributed throughout the year. We assume that olivine immediately dissolves completely, but see section 3.2 for dissolution kinetics.

Six different olivine dissolution scenarios were simulated (table 1). The scenarios differ in (a) the amount of olivine dissolved (1, 3, 10 Pg olivine per year) to investigate any saturation/non-linear effects, (b) the input of either TA, or Si or both to investigate separately the effect on ocean chemistry and on marine biology, and (c) the way olivine is spatially distributed over the ocean. We distinguish between even distribution throughout the whole ocean and a ship-based distribution. The even distribution is not a realistic scenario. Distribution via ships follows the idea of distributing dissolved olivine via ballast water of commercial ships. The NOAA COADS (Comprehensive Ocean–Atmosphere Data Set) data set of monthly SST measurements taken by ships of opportunity (Woodruff *et al* 1998) between 1959–1997 is used to serve as a proxy for ship tracks (figure S3 available at stacks.iop.org/ERL/8/014009/mmedia).

3. Results and discussion

3.1. Simulating open ocean dissolution of olivine

According to our simulation results with REcoM-2 embedded in the MITgcm, the oceanic carbon uptake requires about

Table 1. Description of model runs.

Acronym	Amount Pg olivine per year	What[a]	Spatial distribution[b]
CONTROL	0	–	–
STANDARD	3	Si, TA	Even
STD_SI	3	Si	Even
STD_TA	3	TA	Even
SHIP	3	Si, TA	Ship
SMALL	1	Si, TA	Even
LARGE	10	Si, TA	Even

[a] Distribution of silicate (Si) and/or total alkalinity (TA).
[b] Even: over the global ocean; ship: along ship tracks.

five years to equilibrate to ∼0.29 Pg C per Pg olivine in our STANDARD scenario (figure 1(a)). This scenario assumes an even distribution of 3 Pg of olivine per year over the entire open ocean surface and calculates the effects of both alkalinity and silicic acid input. If not mentioned otherwise results refer to this scenario. Our simulations show that alkalinity input is responsible for 92%, silicic acid input for ∼8% of the carbon sequestration (figure 1(a)). Both effects are cumulative. The carbon sequestration caused by alkalinity is with 0.25 Pg C per Pg olivine 10% smaller than previously assumed with a simpler model (Köhler *et al* 2010).

The addition of silicic acid which accompanies the olivine dissolution improves growing conditions for diatoms
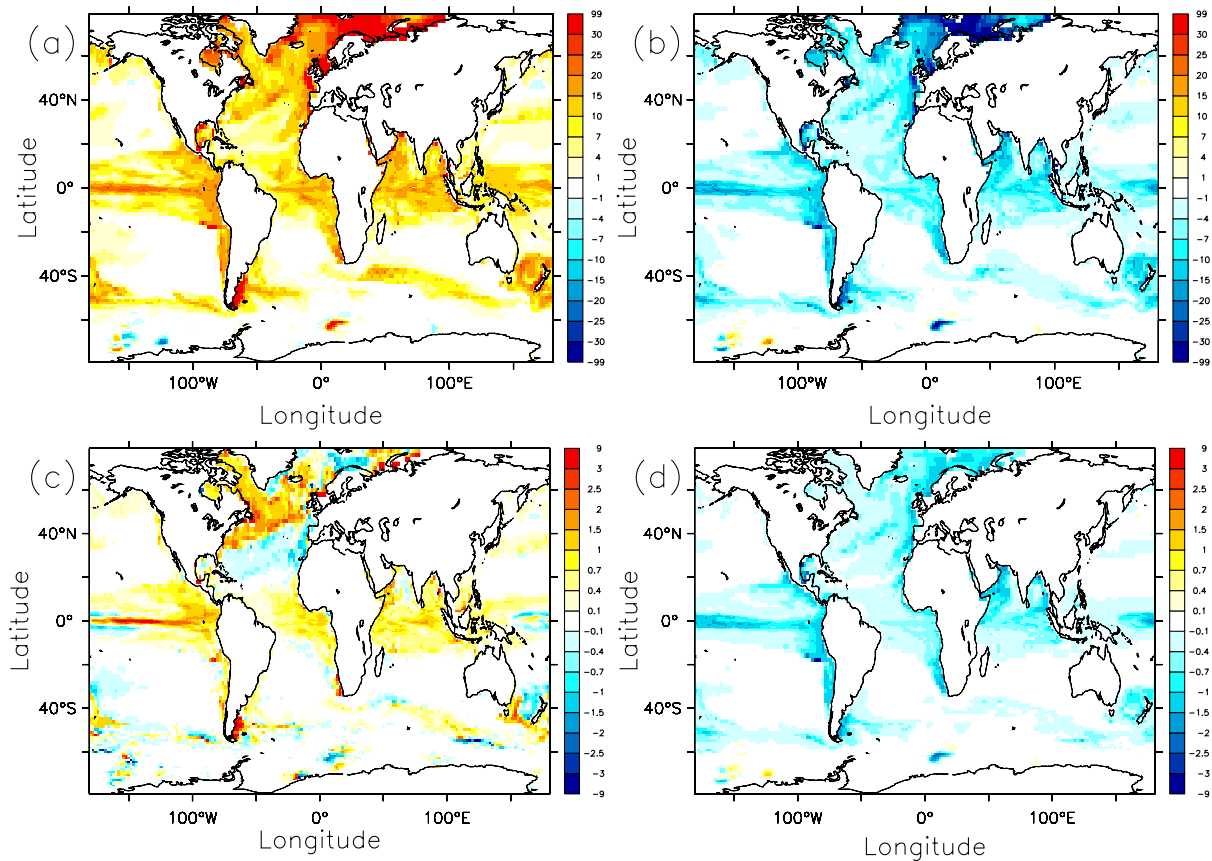
Figure 2. Simulated anomalies (g C (m^2 yr)$^{-1}$) in scenario STANDARD with respect to CONTROL. Shown are annual average in year 2009 (final year). (a) Diatom NPP. (b) Non-diatom NPP. (c) Export production of organic carbon at 87 m depth. (d) CaCO$_3$ export at 87 m depth.

in silicate limited waters. Our model predicts changes in the net primary production (NPP) of diatom and non-diatom species groups. Diatom NPP rises by 2.4 Pg C yr^{-1} (+14%) to 19 Pg C yr^{-1}, while non-diatom NPP shrinks by 1.3 Pg C yr^{-1} (−4%) towards 32 Pg C yr^{-1} (figure 1(b)). Strong seasonal variations in diatom and non-diatom NPP partially compensate each other resulting in a rather constant increase in total NPP by 1 Pg C yr^{-1} (+2%) (figure 1(b)). Consequently, the species shift towards diatoms alters the biological carbon pumps, leading to an increased export of organic matter by about 0.08 Pg C yr^{-1} (+1%) and a decreased export of CaCO$_3$ by the similar amount (−5%) (figure 1(b)). CaCO$_3$ also has a ballasting effect on organic matter export (De La Rocha *et al* 2008). A decrease of CaCO$_3$ export could therefore also lead to a decrease of carbon export, a process which is so far not considered in our study.

There is little biological response to olivine dissolution in the Southern Ocean south of 60°S and throughout most regions of the Southern Hemisphere because of the high natural silicate concentrations there. The diatom NPP (figure 2(a)) increases in the equatorial regime, in the coastal regime, in the North Atlantic, and in the Southern Ocean just north of the opal belt. The maximum increase in both total and diatom NPP occurs in the North Atlantic where there is a low Si:N ratio and in the equatorial regime where silicate is limiting (Dugdale and Wilkerson 1998). The low latitudes

from 20°S to 20°N experience a fairly uniform increase in diatom NPP. Conversely, the average nanophytoplankton NPP (figure 2(b)) was greatly reduced in the areas where diatom NPP was increased. Spatial explicit changes in export production of organic matter and CaCO$_3$ are related to the changes in diatom and non-diatom NPP, respectively (figures 2(c) and (d)).

Olivine dissolution leads to a fairly uniform increase in sea surface pH (figure S4(b) available at stacks.iop.org/ERL/ 8/014009/mmedia) counteracting the ongoing acidification of the surface ocean to some extent. Mean sea surface pH is increased after ten years of olivine dissolution by 0.007 (figure 1(d)), which is to 85% caused by the rise in alkalinity and only to the minor 15% by changes in the marine biology. Changes in carbon uptake, NPP, export production of organic matter and CaCO$_3$, and pH saturate after a few years (figures 1(a), (b), (d)), which makes longer simulations unnecessary. The increase in oceanic carbon uptake with respect to the amount of olivine input is almost linear, with 1, 3, and 10 Pg of olivine addition leading to 0.29, 0.28, and 0.27 Pg C per Pg olivine, respectively (figure 1(c)).

In an alternative distribution scenario SHIP in which olivine input into the surface ocean is weighted by common ship track densities (also called ships of opportunity) very similar results are obtained with some more localized effects on marine biology and pH. While the marine carbon uptake
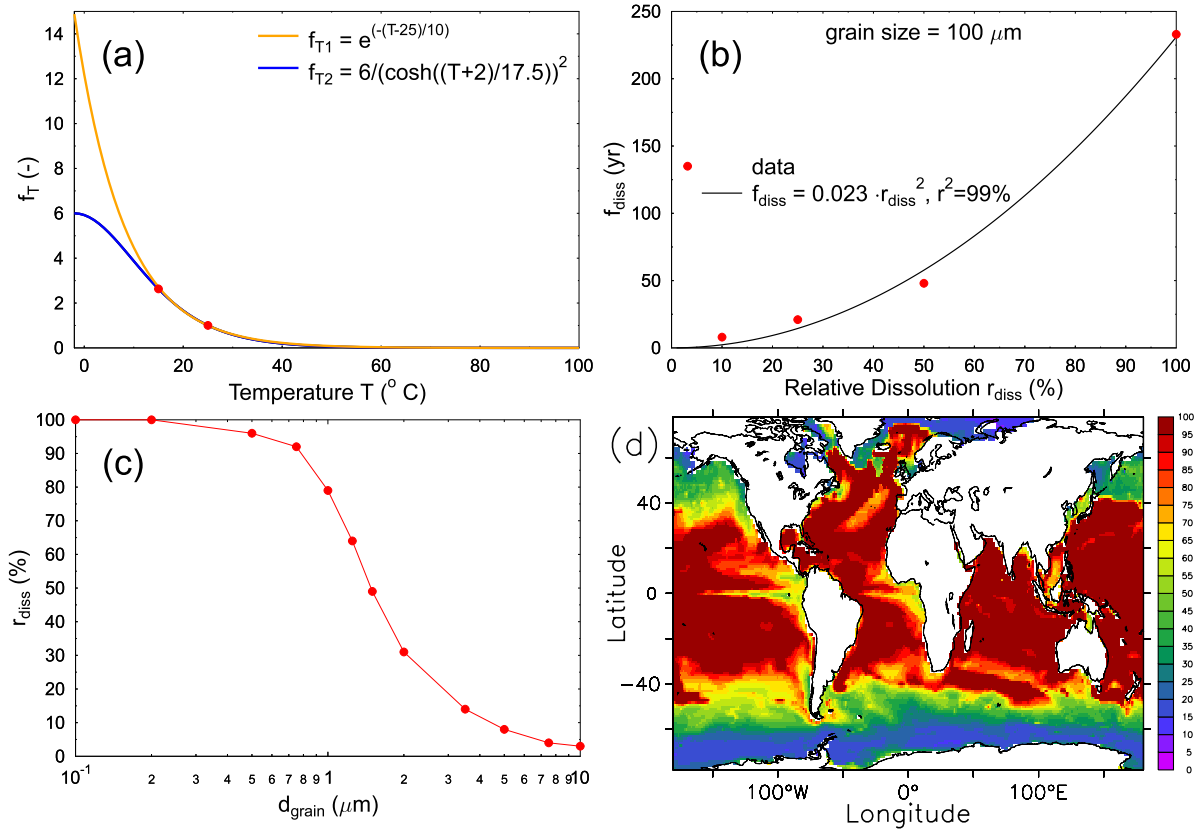
Figure 3. Dissolution kinetics of olivine grains in the surface ocean. (a) Dependency of dissolution from SST (f_T). Two alternative functions for f_T are given. Global results differ by a few percentages only, mainly in cold regions (latitudes higher than 40°). In the following f_{T1} is used. (b) Relationship between relative dissolution r_{diss} and dissolution time f_{diss} for a given grain size of $d_{grain} = 100\ \mu$m. (c) Calculated global mean relative dissolution r_{diss} as function of grain size d_{grain} between 0.1 and 10 μm (log *x*-axis). (d) Calculated relative dissolution r_{diss} for a given grain size d_{grain} of 1 μm as a function of maximum mixed layer depth and SST.

is with 0.28 Pg C per Pg olivine almost identical in SHIP and STANDARD (figure 1(a)), changes in marine biology and sea surface pH are more localized in SHIP. Impacts on the marine biology are now the results of a combination of ship track density pattern with the spatial distribution of silicate limitation (figure S4 available at stacks.iop.org/ERL/8/014009/mmedia). In SHIP changes in sea surface pH are limited to areas north of 40°S, and they are much stronger in the Northern than in the Southern Hemisphere. In the North Atlantic, the impact of olivine dissolution on marine biology is larger in SHIP than in STANDARD because more olivine is dissolved. Marine biology in the North Pacific is not silicate limited, thus both scenarios lead to similar small changes in NPP and export production here. Land-based enhanced weathering (Köhler *et al* 2010) would lead to similar effects localized to river mouths, but the amount of silicic acid reaching the open ocean is unknown because of the extensive anthropogenic alteration of the land–ocean transition (Laruelle *et al* 2009).

3.2. Dissolution kinetics

We calculate the grain size depending dissolution from the residence time in the ocean surface layer and sea surface temperature (SST). For that purpose we generalize previous

findings (Hangx and Spiers 2009), which compiled the dependency of olivine dissolution rate as a function of grain size and temperature. These authors assumed that olivine grains are spherical particles, which dissolve according to a shrinking core model. Using their results we can write the functional dependency of dissolution time (t_{diss} in years), fraction of dissolution after a given time (r_{diss} in %), sea surface temperature (T in °C), and initial grain size (diameter assuming spherical shapes d_{grain} in μm) as

$$t_{diss} = f_{size} \cdot f_T \cdot f_{diss} \qquad (2)$$

$$f_{size} = d_{grain}/(100\ \mu\text{m}) \qquad (3)$$

$$f_{T1} = e^{-((T-25)/10)} \qquad \text{or} \qquad f_{T2} = \frac{6}{\cosh^2(\frac{T+2}{17.5})} \qquad (4)$$

$$f_{diss} = 0.023 \cdot r_{diss}^2. \qquad (5)$$

Briefly, the first factor in equation (2), f_{size}, normalizes to the standard case with grains of 100 μm. Previous results (Hangx and Spiers 2009) depend linearly on initial grain size in the range from 10 to 1000 μm and we here assume its linear extrapolation towards even smaller grain sizes. The second term, f_T, describes the temperature dependency. The dissolution time (Hangx and Spiers 2009) is given for SST of 25 °C (thus $f_{T=25\,°C} = 1$), t_{diss} roughly increases by a factor of 3 when T is reduced from 25 to 15 °C (figure 3(a)).

Uncertainties in dissolution are high for lower temperatures as demonstrated by our suggested two different fitting functions (figure 3(a)). However, this effect is limited to high latitudinal areas and contributes only a few percentages to the global relative dissolution. In the following we will use f_{T1}. The third term in equation (2), f_{diss}, is a second order polynomial fit to the empirically derived dependency between dissolution time and relative dissolution (figure 3(b)). Uncertainties on all these functions are high, at least of the order of 50%. Thus, this exercise should only illustrate the order of magnitude in the dissolution kinetics.

We furthermore estimate the available time for dissolution t_{diss} from the residence time of the olivine particles in the surface mixed layer t_{ML}. We here take the maximum of the monthly means of the surface mixed layer depth D_{ML} calculated in MITgcm, which has a global mean D_{ML} of 64 m. After Stokes law the settling velocity v_{Stokes} due to gravity can be calculated by

$$v_{Stokes} = \frac{2}{9} \cdot \frac{\rho_p - \rho_l}{\mu} \cdot g \cdot \left(\frac{d_{grain}}{2}\right)^2 \qquad (6)$$

with the densities of the olivine particles and the water fluid given by $\rho_p = 3200$ kg m^{-3} and $\rho_l = 1000$ kg m^{-3}, respectively. The dynamic viscosity of water is $\mu = 10^{-3}$ kg (m s)$^{-1}$, $g = 9.81$ m s^{-2} is the gravitational acceleration. We estimate the residence time t_{ML} in the surface mixed layer as $t_{ML} = \frac{D_{ML}}{v_{Stokes}}$.

Our estimate leads to residence times of 3 yr, 10 d or 3 h for olivine particles with grain sizes of 1, 10 or 100 μm, respectively. Accordingly, $\sim$80% of olivine in 1 μm (initial diameter) grains would dissolve before leaving the mixed layer (figure 3(d)), whereas this percentage is already down to 5% for an initial grain size of 10 μm (figure 3(c)). Large particles will eventually dissolve in the deep ocean and not lead to an immediate oceanic carbon uptake. This maximum grain size estimate has also implications for enhanced weathering of olivine on land. If particles are distributed on land they might potentially be transported by winds to open ocean areas. A previous study on land-based enhanced weathering (Köhler *et al* 2010) discussed sequestration efficiency of 10 μm large olivine grains, a size which is easily transported by winds (Müller *et al* 2010). These large grains distributed on land and potentially dispersed by wind to the open ocean will according to our results sink largely undissolved to the deep ocean without the desired short-term carbon sequestration.

The dependences of the dissolution on both SST and mixed layer depth (figure 3(c)) also show that olivine dissolution is only feasible in the latitudinal band between 40°N and 40°S, and additionally in the areas of deep water production in the northern North Atlantic. However, the regions favourable for olivine dissolution largely overlap with commercial shipping tracks, especially in the Atlantic (figures 3(d), S3 available at stacks.iop.org/ERL/8/014009/mmedia) making a distribution scheme based on ships of opportunities a possible option.

Furthermore, scavenging by biogenic particles and physical aggregation, especially at high particle concentrations,

might lead to larger, faster-sinking particles and aggregates. The addition of 3 Pg of olivine (as done in scenario STANDARD) with grain size of 1 μm homogeneously distributed over the world oceans would increase the number density by 10^{11} particles per m^3 in the mixed layer corresponding to 0.4 g olivine m^{-3}. At a grain size of 1 μm and below Brownian motion is the main process driving aggregation. In a recent study (Bressac *et al* 2012) it was shown that adding dust particles of a similar amount (0.8 g m^{-3}) with a somewhat smaller grain size (the number size distribution peaks at 0.1 μm) would lead in a part of the distributed particles to fast particle aggregation resulting in sinking velocities on the order of 50 m d^{-1}. These velocities are orders of magnitude faster than our calculations implying residence times in the surface ocean of rather days than years. The experimental evidence (Bressac *et al* 2012) indicates that our calculated sinking velocities and the estimated fraction of olivine dissolution applies only at low rates of olivine addition.

3.3. General discussion

The sequestration of CO_2 by olivine dissolution is restricted in our study to the immediate effects caused by alkalinity enhancement and ocean fertilization by addition of silicic acid. The transition of CO_2 from the atmosphere to the ocean pools is thus envisaged which might play a role on centennial to millennial timescales. On even longer timescales approaches which guarantee a deposition of C as part of the sediment on the ocean floor might need to be taken into consideration, e.g. using calcium silicates which might precipitate in the form of calcite (Lackner 2002, 2003). Here, other constraints such as source material availability might become important.

Our work shows that open ocean dissolution of olivine is ocean fertilization (Lampitt *et al* 2008). It might also affect oxygen concentration below the surface if more organic matter is respired there. Nowadays $\sim$5% of the ocean volume has hypoxic conditions located in the highly productive equatorial upwelling regions (Matear and Elliott 2004, Lampitt *et al* 2008, Deutsch *et al* 2011). One study (Deutsch *et al* 2011) indicates that low-O_2 waters are prone to further expansion, with the increase in anoxic water generally confined to intermediate waters of the equatorial Indian and Pacific. The olivine dissolution leads to regionally relatively large impacts of up to $\pm$30% in diatom and non-diatom NPP patterns (figures S5(a), (b) available at stacks.iop.org/ERL/8/014009/mmedia), but our simulations show less than a 10% change in regional export production of organic matter (figures S5(c), (d) available at stacks.iop.org/ERL/8/014009/mmedia). In the upwelling regions export production increases by only a few per cent suggesting that the expansion of hypoxic regions due to olivine dissolution might be small.

Olivine dissolution might also lead to a substantial input of iron into the ocean. Its impact on the marine biology might be a subject for future studies. Back-of-the-envelope calculations reveal that an annual dissolution of 3 Pg of olivine with a Mg:Fe ratio of 9:1 is connected with an annual input

of 0.2 Pg Fe. This is an order of magnitude larger than the natural iron input connected with dust deposition (Mahowald *et al* 2005). Because iron solubility (and thus bio-availability) varies by several orders of magnitude between 0.01 and 80% and is not well understood (Baker and Croot 2010), it is not directly clear, what the impact on marine biology would be. Acid processing of aeolian dust particles seems to be an important factor to enhance iron solubility in terrestrial dust (Baker and Croot 2010). As this process is missing in open ocean dissolution of olivine iron solubility from these particles is expected to be on the lower end of the known range. Furthermore, other trace metals found in olivine-containing rocks, e.g. nickel or cadmium (see geochemistry of rocks database GEOROC, http://georoc. mpch-mainz.gwdg.de/georoc), might get dissolved and their effects on marine ecosystems need to be considered.

The suspended olivine density of 0.4 g olivine m^{-3} corresponds to a flux of ∼8 g m^{-2} yr^{-1}. Natural biogenic fluxes, e.g. our calculated export production of organic matter (figure S2(e) available at stacks.iop.org/ERL/ 8/014009/mmedia) range from less than 10 to more than 200 g organic matter m^{-2} yr^{-1} assuming a carbon content of organic matter of 50%. This implies that especially in low-productive open ocean waters of the subtropical region light transparency is expected to be reduced by the olivine input, but—as little NPP or export production occurs there—with only marginal effects on global biological fluxes. In high productivity areas the relative change in the particle flux is on the order of 10%. Global dust deposition in the world oceans is estimated to about 0.5 Pg yr^{-1} (Mahowald *et al* 2005) corresponding to about 1 g m^{-2} yr^{-1}, although the input is spatially very heterogeneous. Furthermore, riverine input of suspended matter is on the order of 20 Pg yr^{-1} (Peucker-Ehrenbrink 2009). The mass concentration of suspended particulate matter in coastal waters around Europe is in the range of 0.02 to 50 g m^{-3} (Babin *et al* 2003). This implies that in coastal waters (so-called 'case 2' waters) natural suspended matter concentrations are for most cases larger than our olivine input rates. All-together, geoengineering large scale distribution of olivine in the open ocean surface waters might have a small negative effect on marine photosynthesis due to shading.

These multiple effects of olivine dissolution on the marine biology—silicic acid input, input of iron and other trace metals, reduced water transparency—would certainly alter our results. The addition of silicic acid added about 10% to the CO_2 uptake, corresponding to 0.1 Pg C yr^{-1} in our STANDARD scenario. The upper limit of CO_2 uptake potential for large scale iron fertilization is in the order of 1 Pg C yr^{-1} (Aumont and Bopp 2006), but 90% of this CO_2 draw down is restricted to the Southern Ocean, where olivine dissolution is according to our results very slow. The combined effect of ocean fertilization by both silicic acid and iron input was so far not investigated and might lead to some surprising synergistic impacts.

The Lloyd's Register Fairplay (Kaluza *et al* 2010) counted in year 2007 16 363 cargo ships and tankers with a total capacity of 665×10^6 gross tonnage (deadweight tonnage DWT). Using an estimate for net tonnage as 50% of DWT

gives a total net tonnage of 0.33 Pg. With an average of 32 ports called per ship per year this gives a total transport capacity of 10 Pg per year. About 100 large ships (net tonnage of 300 000 t each) with a year-round commitment including 32 port calls each would be necessary to distribute 1 Pg of olivine. Alternatively, olivine might be distributed in the ships of opportunity scenario via ballast water, which weighs at least 30% of the DWT of ships running empty (Australian Quarantine and Inspection Service 1993) summing up in the Lloyd Register (Kaluza *et al* 2010) to a global ballast water capacity of 0.2 Pg. Assuming all ships run empty every second run results in an annual ballast water capacity of 3.2 Pg (see also http://globallast.imo.org/ for similar estimates), in which 0.9 Pg of olivine can be dissolved considering that olivine dissolution is limited by the saturation concentration of silicic acid of 2 mmol kg^{-1} (Van Cappellen and Qiu 1997) derived from biogenic silica reactivity. However, we like to emphasize that the estimation of this limitation is subject to uncertainty, because direct olivine dissolution rates available to us were so far obtained for silicic acid concentration below 1 mmol kg^{-1}, thus at least a factor of 2 below its saturation concentration (Oelkers 2001, Pokrovsky and Schott 2000, Rimstidt *et al* 2012), although the decline of olivine dissolution rates for rising silicic acid concentrations (Pokrovsky and Schott 2000) hints already at a saturation effect.

Grinding particles to 1 μm grain size is a practical challenge which consumes by far the most energy in the whole processing chain, at least an order of magnitude more than mining and transport (Hangx and Spiers 2009, Köhler *et al* 2010, Renforth 2012). Energy costs for grinding 80% of the particles down to 1 μm with present day technology are as high as 300–350 kWh t^{-1} (Renforth 2012). Depending on the type of energy production (Rubin *et al* 2007) this might release as much as 350 (gas) to 800 (coal) g of CO_2 per kWh reducing carbon sequestration efficiency by up to 30%.

Implementation of enhanced weathering would require an operation on a global scale that will bring olivine mining to one of the world's largest mining sector (Schuiling and Krijgsman 2006, Mohr and Evans 2009). CO_2 and other greenhouse gases produced by grinding, mining, and transport of olivine would offset sequestration capacity of enhanced weathering. An estimate (Köhler *et al* 2010) assuming local mining and restricted transport (less than 1000 km and mainly by ships) for the total CO_2 expenditure is close to 10%, which gives a carbon sequestration efficiency of 90%. This does not include the fuel required for ships that would distribute olivine nor the energy demand necessary for grinding to small grain sizes of 1 μm as calculated above. If they are included, carbon sequestration efficiency falls below 60% and makes open ocean dissolution of olivine a rather inefficient geoengineering technique.

Our results show that enhanced weathering might help to reduce atmospheric CO_2. However, with a carbon uptake rate of 0.28 g carbon per g of olivine (neglecting reduced efficiency as discussed above) the recent fossil emissions of about 9 Pg C yr^{-1} (Peters *et al* 2012) are difficult if not impossible to be reduced solely based on olivine dissolution. An upper limit for the open ocean distribution

of olivine is difficult to estimate, but such a limit certainly depends on shipping capacities, exploitation of olivine, and low distribution rates to prevent particle aggregation. In our STANDARD scenario (3 Pg of olivine dissolution per year) about 9% of the anthropogenic CO_2 emissions would be compensated. This is slightly higher than the compensation rate of about 7% after ten years of implementation for the ongoing surface ocean acidification of nowadays 0.1 pH-units (Doney *et al* 2009).

4. Conclusions

In conclusion, our study provides a general picture of the intended and some of the unintended effects of open ocean dissolution of olivine on atmospheric CO_2, surface ocean pH, and marine biology. Most challenging is the necessity to grind olivine to grain sizes of the order of 1 μm to enable dissolution before sinking out of the surface mixed layer. This size limitation is also of relevance for wind dispersed olivine distributed on land. Energy consumption for grinding will reduce the CO_2 sequestration efficiency significantly. It needs about 100 large dedicated ships to distribute 1 Pg of olivine per year over a large ocean surface area. Alternatively, the distribution of olivine in ballast water of the fleet of commercial ships is an option which has the potential to distribute up to 0.9 Pg of olivine per year. Additionally, most shipping tracks lie in regions favourable for olivine dissolution. There are two cumulative mechanisms which contribute to the sequestration of carbon with the majority ($\sim$92%) caused by ocean chemistry changes due to alkalinity input and a minority ($\sim$8%) by the changes in species composition and the biological carbon pumps due to silicic acid input. Marine biology might be further influenced by the input of trace metals, e.g. Fe or Ni, and reduced light availability connected with the olivine dissolution. The alkalinity input counteracts the ongoing acidification of the surface ocean. Land-based enhanced weathering of olivine might lead to similar changes in marine biology (but more localized to river mouths) depending on the amount of silicic acid reaching the open ocean via rivers.

Acknowledgments

References

Aumont O and Bopp L 2006 Globalizing results from ocean *in situ* iron fertilization studies *Glob. Biogeochem. Cycles* **20** GB2017

Aumont O, Orr J C, Monfray P, Madec G and Maier-Reimer E 1999 Nutrient trapping in the equatorial Pacific: the ocean circulation solution *Glob. Biogeochem. Cycles* **13** 351–69

Australian Quarantine and Inspection Service 1993 *Ballast Water Management* (*Ballast Water Research Series* vol 4) (Canberra: Australian Goverment Publishing Service)

Babin M, Stramski D, Ferrari G M, Claustre H, Bricaud A, Obolensky G and Hoepffner N 2003 Variations in the light absorption coefficients of phytoplankton, nonalgal particles, and dissolved organic matter in coastal waters around Europe *J. Geophys. Res.* **108** 3211

Baker A and Croot P 2010 Atmospheric and marine controls on aerosol iron solubility in seawater *Marine Chem.* **120** 4–13

Berner R A 1990 Atmospheric carbon dioxide levels over Phanerozoic time *Science* **249** 1382–6

Beusen A H W, Bouwman A F, Dürr H H, Dekkers A L M and Hartmann J 2009 Global patterns of dissolved silica export to the coastal zone: Results from a spatially explicit global model *Glob. Biogeochem. Cycles* **23** GB0A02

Bressac M, Guieu C, Doxaran D, Bourrin F, Obolensky G and Grisoni J M 2012 A mesocosm experiment coupled with optical measurements to assess the fate and sinking of atmospheric particles in clear oligotrophic waters *Geo-Marine Lett.* **32** 153–64

Caldeira K and Rau G H 2000 Accelerating carbonate dissolution to sequester carbon dioxide in the ocean: geochemical implications *Geophys. Res. Lett.* **27** 225–8

De La Rocha C L, Nowald N and Passow U 2008 Interactions between diatom aggregates, minerals, particulate organic carbon, and dissolved organic matter: further implications for the ballast hypothesis *Glob. Biogeochem. Cycles* **22** GB4005

Deer W, Howie R and Zussman J 1992 *An Introduction to the Rock-Forming Minerals* 2nd edn (Harlow: Longman)

Deutsch C, Brix H, Ito T, Frenzel H and Thompson L 2011 Climate-forced variability of ocean hypoxia *Science* **333** 336–9

Doney S C, Fabry V J, Feely R A and Kleypas J A 2009 Ocean acidification: the other CO_2 problem *Ann. Rev. Marine Sci.* **1** 169–92

Dugdale R C and Wilkerson F P 1998 Silicate regulation of new production in the equatorial Pacific upwelling *Nature* **391** 270–3

Enting I, Wigley T and Heimann M 1994 Future emissions and concentrations of carbon dioxide: Key ocean/atmosphere/land analyses *Technical Report 31* (Melbourne: CSIRO Division of Atmospheric Research)

Friedlingstein P, Solomon S, Plattner G K, Knutti R, Ciais P and Raupach M R 2011 Long-term climate implications of twenty-first century options for carbon dioxide emission mitigation *Nature Clim. Change* **1** 457–61

Geider R J, MacIntyre H L and Kana T M 1998 A dynamic regulatory model of phytoplanktonic acclimation to light, nutrients, and temperature *Limnol. Oceanogr.* **43** 679–94

Hangx S J and Spiers C J 2009 Coastal spreading of olivine to control atmospheric CO_2 concentrations: a critical analysis of viability *Int. J. Greenhouse Gas Control* **3** 757–67

Harvey L D D 2008 Mitigating the atmospheric CO_2 increase and ocean acidification by adding limestone powder to upwelling regions *J. Geophys. Res.* **113** C04028

Hauck J 2012 Processes in the Southern Ocean carbon cycle: dissolution of carbonate sediments and inter-annual variability of carbon fluxes *PhD Thesis* University of Bremen (http://hdl. handle.net/10013/epic.39964.d001)

Joshi M, Hawkins E, Sutton R, Lowe J and Frame D 2011 Projections of when temperature change will exceed 2 °C above pre-industrial levels *Nature Clim. Change* **1** 407–12

Kalnay E *et al* 1996 The NCEP/NCAR 40-year reanalysis project *Bull. Am. Meteorol. Soc.* **77** 437–71

Kaluza P, Kölzsch A, Gastner M T and Blasius B 2010 The complex network of global cargo ship movements *J. R. Soc. Interface* **7** 1093–103

Keeling R, Piper S, Bollenbacher A and Walker J 2009 Atmospheric CO_2 records from sites in the SIO air sampling network *Trends: A Compendium of Data on Global Change* (Oak Ridge, TN: Carbon Dioxide Information Analysis Center, Oak Ridge National Laboratory, US Department of Energy) (doi:10.3334/CDIAC/atg.035)

Kheshgi H S 1995 Sequestering atmospheric carbon dioxide by increasing ocean alkalinity *Energy* **20** 915–22

Köhler P, Hartmann J and Wolf-Gladrow D A 2010 Geoengineering potential of artificially enhanced silicate weathering of olivine *Proc. Natl Acad. Sci.* **107** 20228–33

Lackner K S 2002 Carbonate chemistry for sequestering fossil carbon *Ann. Rev. Energy Environ.* **27** 193–232

Lackner K S 2003 A guide to CO_2 sequestration *Science* **300** 1677–8

Lampitt R *et al* 2008 Ocean fertilization: a potential means of geoengineering? *Phil. Trans. R. Soc.* A **366** 3919–45

Large W and Yeager S 2008 The global climatology of an interannually varying air-sea flux data set *Clim. Dynam.* **33** 341–64

Laruelle G G *et al* 2009 Anthropogenic perturbations of the silicon cycle at the global scale: key role of the land–ocean transition *Glob. Biogeochem. Cycles* **23** GB4031

Lenton T M and Vaughan N E 2009 The radiative forcing potential of different climate geoengineering options *Atmos. Chem. Phys.* **9** 5539–61

Losch M, Menemenlis D, Campin J M, Heimbach P and Hill C 2010 On the formulation of sea-ice models. Part 1: effects of different solver implementations and parameterizations *Ocean Model.* **33** 129–44

Mahowald N M, Baker A R, Bergametti G, Brooks N, Duce R A, Jickells T D, Kubilay N, Prospero J M and Tegen I 2005 Atmospheric global dust cycle and iron inputs to the ocean *Glob. Biogeochem. Cycles* **19** GB4025

Marshall J, Adcroft A, Holl C, Perelman L and Heisey C 1997 A finite-volume, incompressible Navier–Stokes model for studies of the ocean on parallel computers *J. Geophys. Res.* **102** 5753–66

Matear R J and Elliott B 2004 Enhancement of oceanic uptake of anthropogenic CO_2 by macronutirent fertilization *J. Geophys. Res.* **109** C04001

Meinshausen M, Meinshausen N, Hare W, Raper S C B, Frieler K, Knutti R, Frame D J and Allen M R 2009 Greenhouse-gas emission targets for limiting global warming to 2 °C *Nature* **458** 1158–62

Mohr S and Evans G 2009 Forecasting coal production until 2100 *Fuel* **88** 2059–67

Müller K, Lehmann S, van Pinxteren D, Gnauk T, Niedermeier N, Wiedensohler A and Herrmann H 2010 Particle characterization at the Cape Verde atmospheric observatory during the 2007 RHaMBLe intensive *Atmos. Chem. Phys.* **10** 2709–21

Neftel A, Moor E, Oeschger H and Stauffer B 1985 Evidence from polar ice cores for the increase in atmospheric CO_2 in the past two centuries *Nature* **315** 45–7

Nelson D M, Tréguer P, Brzezinski M A, Leynaert A and Quéguiner B 1995 Production and dissolution of biogenic silica in the ocean: revised global estimates, comparison with regional data and relationship to biogenic sedimentation *Glob. Biogeochem. Cycles* **9** 359–72

Oelkers E H 2001 An experimental study of forsterite dissolution rates as a function of temperature and aqueous Mg and Si concentrations *Chem. Geology* **175** 485–94

Peters G P, Marland G, Le Quéré C, Boden T, Canadell J G and Raupach M R 2012 Rapid growth in CO_2 emissions after the 2008–2009 global financial crisis *Nature Clim. Change* **2** 2–4

Peucker-Ehrenbrink B 2009 Land2Sea database of river drainage basin sizes, annual water discharges, and suspended sediment fluxes *Geochem. Geophys. Geosyst.* **10** Q06014

Pokrovsky O S and Schott J 2000 Forsterite surface composition in aqueous solutions: a combined potentiometric, electrokinetic, and spectroscopic approach *Geochim. Cosmochim. Acta* **64** 3299–312

Ragueneau O, Schultes S, Bidle K, Claquin P and Moriceau B 2006 Si and C interactions in the world ocean: importance of ecological processes and implications for the role of diatoms in the biological pump *Glob. Biogeochem. Cycles* **20** GB4S02

Rau G H 2008 Electrochemical splitting of calcium carbonate to increase solution alkalinity: implications for mitigation of carbon dioxide and ocean acidity *Environ. Sci. Technol.* **42** 8935–40

Rau G H 2011 CO_2 mitigation via capture and chemical conversion in seawater *Environ. Sci. Technol.* **45** 1088–92

Renforth P 2012 The potential of enhanced weathering in the UK *Int. J. Greenhouse Gas Control* **10** 229–43

Rimstidt J D, Brantley S L and Olsen A A 2012 Systematic review of forsterite dissolution rate data *Geochim. Cosmochim. Acta* **99** 159–78

Rogelj J, Hare W, Lowe J, van Vuuren D P, Riahi K, Matthews B, Hanaoka T, Jiang K and Meinshausen M 2011 Emission pathways consistent with a 2 °C global temperature limit *Nature Clim. Change* **1** 413–8

Rubin E S, Chen C and Rao A B 2007 Cost and performance of fossil fuel power plants with CO_2 capture and storage *Energy Policy* **35** 4444–54

Schartau M, Engel A, Schröter J, Thoms S, Völker C and Wolf-Gladrow D 2007 Modelling carbon overconsumption and the formation of extracellular particulate organic carbon *Biogeosciences* **4** 433–54

Schuiling R D and Krijgsman P 2006 Enhanced weathering: an effective and cheap tool to sequester CO_2 *Clim. Change* **74** 349–54

Solomon S, Plattner G K, Knutti R and Friedlingstein P 2009 Irreversible climate change due to carbon dioxide emissions *Proc. Natl Acad. Sci.* **106** 1704–9

The Royal Society 2009 *Geoengineering the Climate: Science, Governance and Uncertainty* (London: The Royal Society) (www.royalsoc.ac.uk)

Tréguer P J and De La Rocha C L 2013 The world ocean silica cycle *Ann. Rev. Marine Sci.* **5** 477–501

UNFCCC 2009 *Copenhagen Accord* (New York: United Nations) (http://unfccc.int/resource/docs/2009/cop15/eng/l07.pdf)

Van Cappellen P and Qiu L 1997 Biogenic silica dissolution in sediments of the Southern Ocean. I. Solubility *Deep Sea Res. II: Topical Studies in Oceanography* **44** 1109–28

Williamson P and Turley C 2012 Ocean acidification in a geoengineering context *Phil. Trans. R. Soc. A: Math., Phys. Eng. Sci.* **370** 4317–42

Woodruff S, Diaz H, Elms J and Worley S 1998 COADS Release 2 data and metadata enhancements for improvements of marine surface flux fields *Phys. Chem. Earth* **23** 517–26

Zeebe R E and Wolf-Gladrow D A 2001 CO_2 *in Seawater: Equilibrium, Kinetics, Isotopes* (*Elsevier Oceanography Book Series* vol 65) (Amsterdam: Elsevier)

Supplementary Information to

Geoengineering impact of open ocean dissolution of olivine on atmospheric CO_2, surface ocean pH and marine biology

P. Köhler, J.F. Abrams, C. Völker, J. Hauck, D.A. Wolf-Gladrow

Supplementary Text: Control run

We limit our analysis of the CONTROL run here to those variables for which we discuss the changes brought about by olivine input, the full model validation will be published elsewhere.

After 100 years of spin-up important variables of the marine biology (e.g. NPP, export production) show some inter-annual variability that is mostly driven by the inter-annually varying atmospheric forcing, but no long-term trends are evident. Globally NPP is relatively constant with 50.1 Pg C yr^{-1} in the final year, which is in the range of current satellite-based estimates (Carr et al. 2006). Diatoms account for 33% of the total NPP, while non-diatom species account for the other 67%. The export fluxes of organic carbon, of $CaCO_3$ and of biogenic silica are 10.7 Pg C yr^{-1}, 1.4 Pg C yr^{-1} and 104 Tmol Si yr^{-1}, respectively, roughly in line with data-based estimates (Schlitzer 2000, Berelson et al. 2007, Tréguer 2002).

The spatial patterns of the annual average of both total and diatom NPP show maxima in coastal and equatorial upwelling regions, in sub-polar gyres and around the Antarctic Circumpolar Current (figures S2(a),(b)). In the subtropical gyres, diatom NPP is very small, while non-diatom NPP is more evenly distributed with a weaker maximum near the equator and a minimum in the Southern Ocean (figures S2(b),(c)) Except for areas with strong fresh-water influence, surface pH is relatively constant around 8.05, with somewhat higher values reached in the sub-polar North Atlantic and Pacific (figures S2(d)). Organic carbon export out of the euphotic zone is concentrated in the areas of highest NPP and there is very little export in the subtropical gyres (figure S2(e)). The carbon export production in the equatorial Pacific is likely too strong, a known feature of biogeochemical models with coarse resolution (Aumont et al. 1999). Export of $CaCO_3$ is more homogeneous and reflects mostly the small phytoplankton NPP (figure S2(f)). Overall, the model gives similar spatial patterns in biological activity to other typical global biogeochemical models (Gehlen et al. 2006, Schneider et al. 2008, Steinacher et al. 2010).

The net oceanic carbon uptake in the final simulated year 2009 is 1.5 Pg C yr^{-1}. This is at the lower end of estimates of annual contemporary carbon uptake (Gruber et al. 2009), but it most

likely also contains some contribution from the long-term adjustment of deep tracer fields, that have not come into equilibrium with atmospheric physical forcings yet after 110 simulated years. As we are focusing here mainly on differences between CONTROL and sensitivity runs, these effects should have only a marginal effect on our results.

Supplementary References

Aumont O, Orr J C, Monfray P, Madec G & Maier-Reimer E 1999 Nutrient trapping in the equatorial Pacific: The ocean circulation solution *Global Biogeochemical Cycles* **13**, 351–369.

Berelson W M, Balch W M, Najjar R, Feely R A, Sabine C & Lee K 2007 Relating estimates of $CaCO_3$ production, export, and dissolution in the water column to measurements of $CaCO_3$ rain into sediment traps and dissolution on the sea floor: a revised global carbonate budget *Global Biogeochemical Cycles* **21**, GB1024, doi: 10.1029/2006GB002803.

Carr M E, Friedrichs M A M, Schmeltz M, Aita M N, Antoine D, Arrigo K R, Asanuma I, Aumont O, Barber R, Behrenfeld M, Bidigare R, Buitenhuis E T, Campbell J, Ciotti A, Dierssen H, Dowell M, Dunne J, Esaias W, Gentili B, Gregg W, Groom S, Hoepffner N, Ishizaka J, Kameda T, Le Quere C, Lohrenz S, Marra J, Melin F, Moore K, Morel A, Reddy T E, Ryan J, Scardi M, Smyth T, Turpie K, Tilstone G, Waters K & Yamanaka Y 2006 A comparison of global estimates of marine primary production from ocean color *Deep-Sea Research Part II, Topical Studies In Oceanography* **53**(5-7), 741–770.

Gehlen M, Bopp L, Emprin N, Aumont O, Heinze C & Ragueneau O 2006 Reconciling surface ocean productivity, export fluxes and sediment composition in a global biogeochemical ocean model *Biogeosciences* **3**(4), 521–537.

Gruber N, Gloor M, Mikaloff Fletcher S E, doney S C, Dutkiewicz S, Follows M J, Gerber M, Jacobson A R, Joos F, Lindsay K, Menemenlis D, Mouchet A, Müller S A, Sarmiento J L & Takahashi T 2009 Oceanic sources, sinks, and transport of atmospheric CO_2 *Global Biogeochemical Cycles* **23**, GB1005, doi: 10.1029/2008GB003349.

Schlitzer R 2000 Applying the adjoint method for biogeochemical modelling: export of particulate organic matter in the world ocean *in* P Kasibhatla, M Heimann, P Rayner, N Mahowald, R. G

Prinn & D. E Hartley, eds, 'Inverse methods in Global Biogeochemical Cycles' Vol. 114 of *Geophysical Monographs* AGU Washington, D.C. pp. 107–124.

Schneider B, Bopp L, Gehlen M, Segschneider J, Frölicher T L, Cadule P, Friedlingstein P, Doney S C, Behrenfeld M J & Joos F 2008 Climate-induced interannual variability of marine primary and export production in three global coupled climate carbon cycle models *Biogeosciences* **5**(2), 597–614.

Steinacher M, Joos F, Frölicher T L, Bopp L, Cadule P, Cocco V, Doney S C, Gehlen M, Lindsay K, Moore J K, Schneider B & Segschneider J 2010 Projected 21st century decrease in marine productivity: a multi-model analysis *Biogeosciences* **7**(3), 979–1005.

Tréguer P 2002 Silica and the cycle of carbon in the ocean *Comptes Rendus Geoscience* **334**(1), 3–11.

Woodruff S, Diaz H, Elms J & Worley S 1998 COADS Release 2 data and metadata enhancements for improvements of marine surface flux fields *Physics and Chemistry of The Earth* **23**, 517–526.
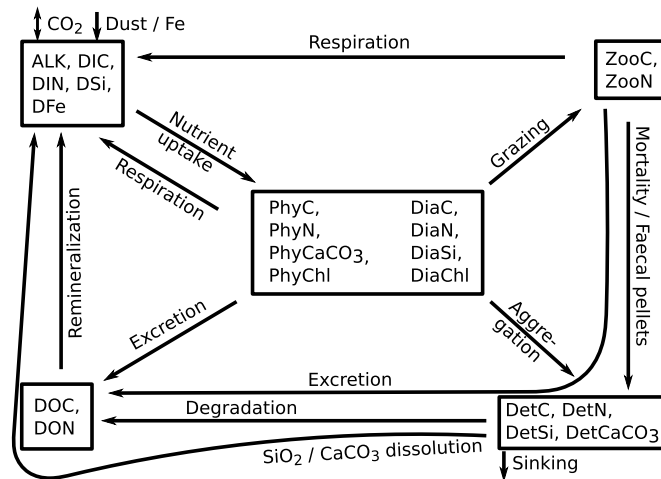
Figure S 1: The REcoM-2 schematic diagram shows the compartments and inter-compartmental fluxes of the upper mixed layer ecosystem. The model includes various dissolved inorganic species, namely carbon (DIC), nitrogen (DIN), iron (DFe) and silicon (DSi), as well as total alkalinity (ALK). These species are used by two different phytoplankton groups (diatoms (Dia) and non-diatoms (Phy)). In the phytoplankton pools of chlorophyll (Chl), carbon (C) and nitrogen (N) are monitored. Additionally, in diatoms pools of silicate (Si) and in non-diatoms of calcium carbonate ($CaCO_3$) are calculated. Zooplankton (Zoo) grazes on phytoplankton. For zooplankton, the cycling of carbon and nitrogen is included. Mortality of phytoplankton and zooplankton leads to detrital forms of nitrogen, carbon, silicon, and calcium carbonate. Detritus (Det) sinks (export production). Via excretion and degradation dissolved organic carbon (DOC) and nitrogen (DON) pools are filled. Dissolution and remineralisation finally lead back to the dissolved inorganic species.
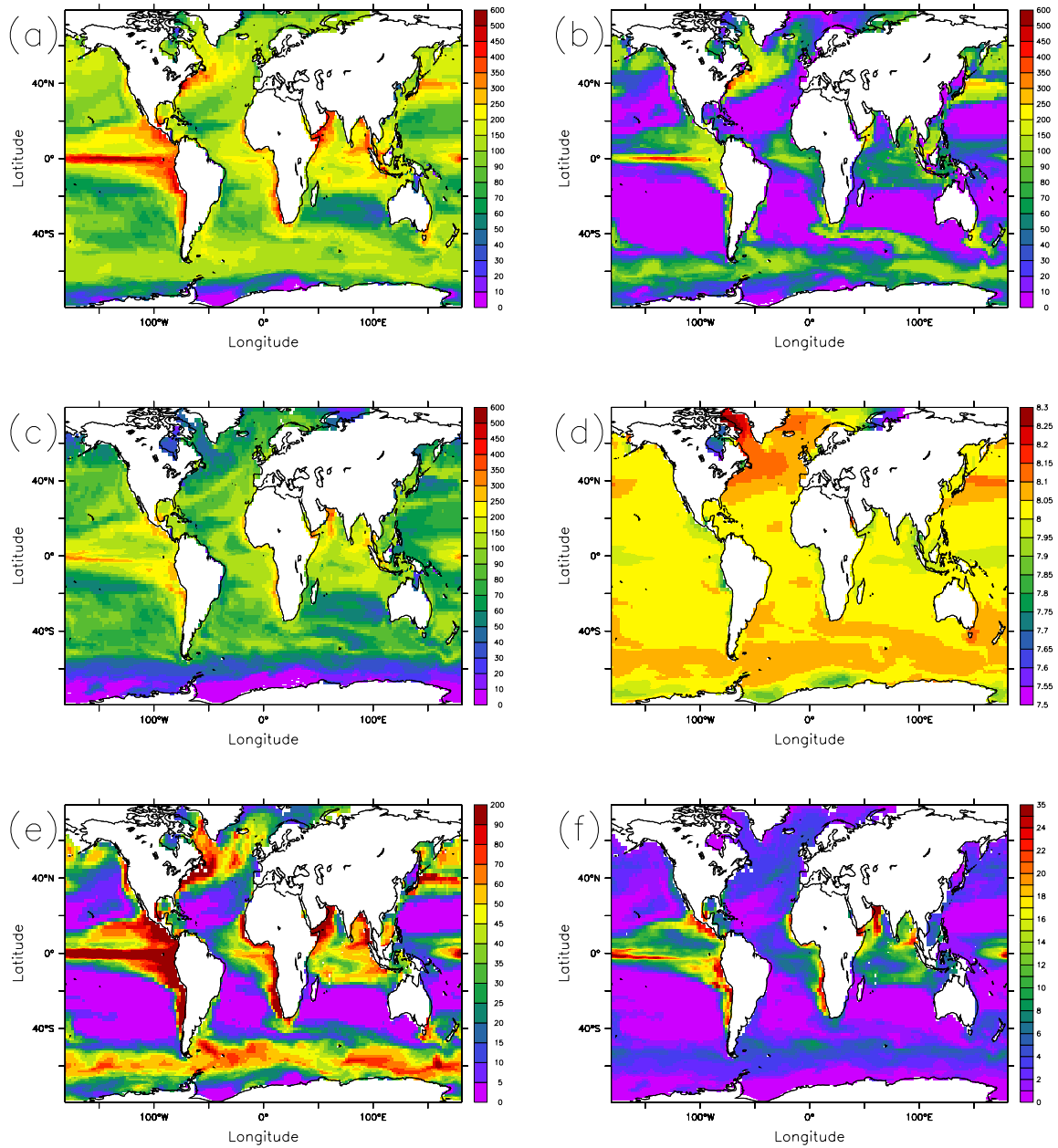
4

Figure S 2: CONTROL run. Annual mean values in the final simulated year (2009). (a) Total NPP. (b) Diatom NPP. (c) Non-diatom NPP. (d) Sea surface pH. (e) Export production of organic carbon at 87 m depth. (f) CaCO$_3$ export at 87 m depth. Units are (g C (m^2 yr)$^{-1}$) apart from (d), which is (-).
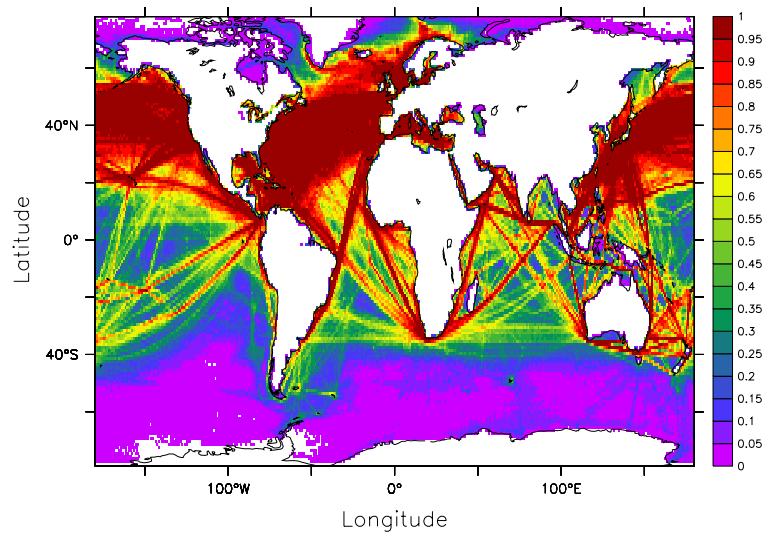
Figure S 3: Normalized ship track density derived from NOAA COADS data set of SST (Woodruff et al. 1998) taken between 1959 and 1992.
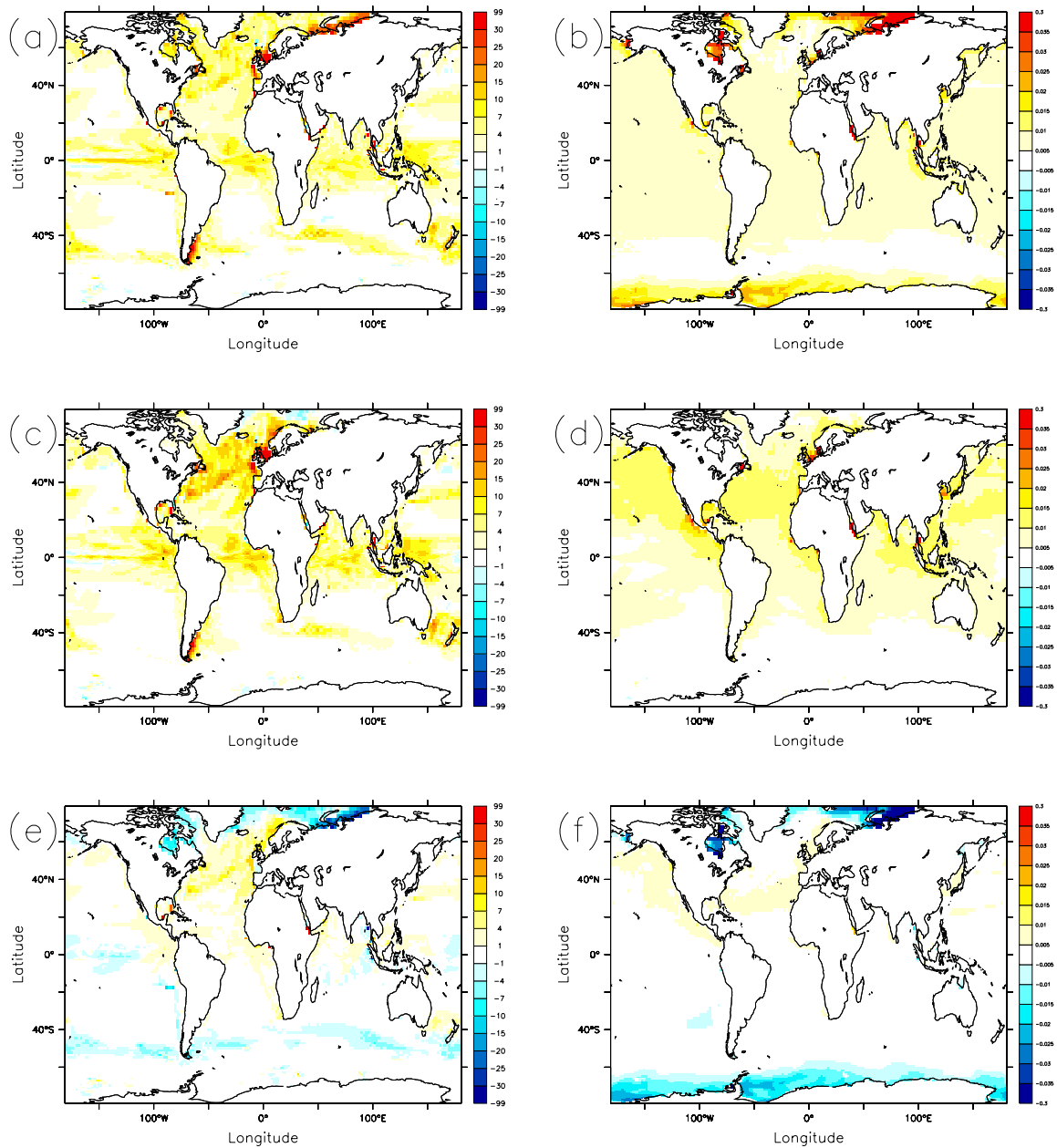
Figure S 4: Simulated anomalies in total NPP (left) and sea surface pH (right) for scenarios STANDARD and SHIP. Global surface maps of annual mean values in the final simulated year (2009). Total NPP anomaly in (a) STANDARD vs. CONTROL and (c) SHIP vs. CONTROL. Sea surface pH anomaly in (b) STANDARD vs. CONTROL and (d) SHIP vs. CONTROL. (e) Total NPP (SHIP vs. STANDARD). (f) Sea surface pH (SHIP vs. STANDARD). Units in (a), (c) and (e) are (g C $(m^2\ yr)^{-1}$) and in (b), (d), and (f) are (-).
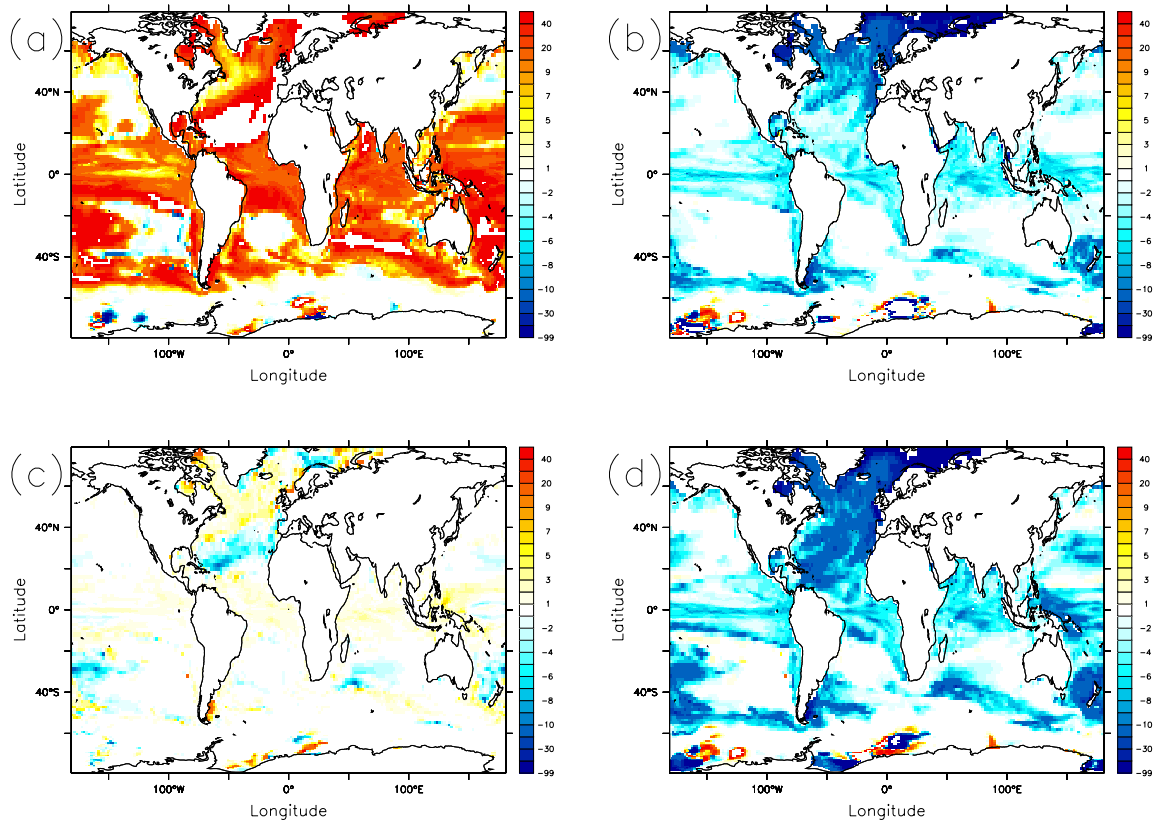
Figure S 5: Relative changes (in %) in scenario STANDARD with respect to CONTROL. Global surface maps of annual mean values in the final simulated year (2009). (a) Non-diatom NPP, (b) diatom NPP, (c) export production of organic matter and (d) $CaCO_3$ export.